

Multi-Scale Investigation of the Performance of Limestone in Concrete

Dale P. Bentz^{1*}, Ahmad Ardani², Tim Barrett³, Scott Z. Jones¹, Didier Lootens⁴, Max A. Peltz¹, Taijiro Sato⁵, Paul E. Stutzman,¹ Jussara Tanesi⁶, and W. Jason Weiss³

*corresponding author, Phone: (301)975-5865

¹National Institute of Standards and Technology
100 Bureau Drive, Stop 8615
Gaithersburg, MD 20899 USA

E-mail: dale.bentz@nist.gov, scott.jones@nist.gov, max.peltz@nist.gov,
paul.stutzman@nist.gov

^{2,6}Turner-Fairbanks Highway Research Center
6300 Georgetown Pike
McLean VA 22101 USA

²Federal Highway Administration
E-mail: ahmad.ardani@dot.gov

⁶SES Group and Associates
E-mail: jussara.tanesi.ctr@dot.gov

³Department of Civil Engineering
Purdue University
West Lafayette, IN 47907 USA
E-mail: barrett1@purdue.edu, wjweiss@purdue.edu

⁴Sika Technology AG - Central Research
Tueffenwies 16
CH-8048 Zurich SWITZERLAND
E-mail: lootens.didier@ch.sika.com

⁵National Research Council Canada
1200 Montreal Road, M-20
Ottawa, Ontario K1A 0R6 CANADA
E-mail: taijiro.sato@nrc-cnrc.gc.ca

Abstract

Limestone (calcium carbonate, CaCO₃) has long been a critical component of concrete, whether as the primary raw material for cement production, a fine powder added to the binder component, or a source of fine and/or coarse aggregate. This paper focuses on the latter two of these examples, providing a multi-scale investigation of the influences of both fine limestone powder and conventional limestone aggregates on concrete performance. Fine limestone powder in the form of calcite provides a favorable surface for the nucleation and growth of calcium silicate hydrate gel at early ages, accelerating and amplifying silicate hydration, and a source of carbonate ions to participate in reactions with the aluminate phases present in the cement (and fly

ash). Conversely, the aragonite polymorph of CaCO_3 exhibits a different crystal (and surface) structure and therefore neither accelerates nor amplifies silicate hydration at a similar particle size/surface area. However, because these two forms of CaCO_3 have similar solubilities in water, the aragonite does contribute to an enhancement in the reactivity of the aluminate phases in the investigated systems, chiefly via carboaluminate formation. In 100 % ordinary portland cement (OPC) concretes, 10 % of the OPC by volume can be replaced with an equivalent volume of limestone powder, while maintaining acceptable performance. A comparison between limestone and siliceous aggregates indicates that the former often provide higher measured compressive strengths at equivalent levels of hydration, even when the two aggregate types exhibit similar elastic moduli. This suggests that the interfacial transition zone in the limestone-based concretes exhibits a higher degree of bonding, likely due to the favorable physical (texture) and chemical nature of the limestone surfaces. These observations reinforce the value of utilizing limestone to increase the performance and sustainability of 21st century concrete construction.

Keywords: Aggregate; aragonite; calcite; heat release; hydration; limestone; precipitation; setting; strength.

Introduction

The 21st century sustainability movement in North America has produced increased interest in replacing a portion of the ordinary portland cement (OPC) in concrete with limestone powder, thus reducing both the CO_2 and energy footprints of the concrete. While portland limestone cements (PLC) have been used in Europe for many years, it is only recently that U.S. standards have first permitted the incorporation of up to 5 % (inter)ground limestone in ASTM C150 portland cement [1] and subsequently introduced a new class of PLCs into ASTM C595 [2], the standard for blended cements, with the U.S. revisions following after the Canadian implementation in both cases. Type IL in ASTM C595 permits the incorporation of up to 15 % limestone by mass in the blended cement. The performance equivalence of these PLC-IL cements with ASTM C150 cements has been recently documented in a series of technical articles [3-7]. As these new PLCs continue to establish market acceptance, a viable alternative to an interground blended cement is the direct addition of a limestone powder to an ASTM C150 cement at the ready-mix or pre-cast production plant, similar to the manner in which slag, fly ash (FA), or silica fume are often introduced by the concrete manufacturer. Since the limestone and cement are processed separately in this case, the particle characteristics (surface area, particle size) of each can be accurately characterized and controlled, and investigations of how these characteristics affect performance in cement-based materials can be conveniently performed [8-12]. These studies have revealed the importance of limestone powder surface area (fineness) in boosting early-age hydration and reducing initial and final setting times, particularly in ternary blends containing fly ash at conventional or high-volume addition rates. The viability of this approach is further reinforced by the ongoing development of a ground limestone (and mineral filler) proportioning guide and a materials specification within ACI and ASTM, respectively.

A variety of potential ternary mixtures of cement, fly ash, and limestone powder are represented in Figure 1. Because the efficacy of fine limestone powders to improve the setting times and mechanical and transport properties of high-volume fly ash (HVFA) mixtures has been investigated extensively [10,11], the present study focuses on two other types of mixtures, as indicated by the three filled diamond data points in Figure 1. The two data points on the bottom

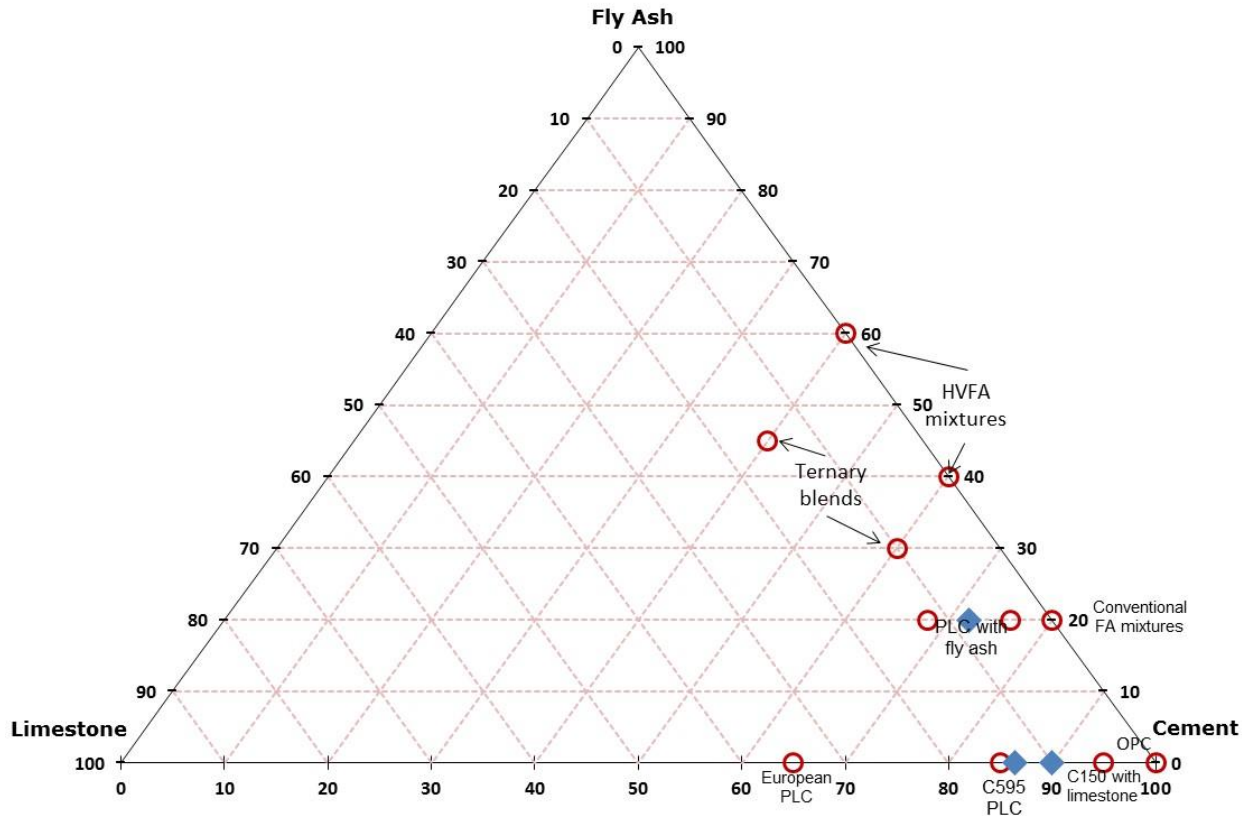


Figure 1. Ternary plot indicating common mixtures of cement, fly ash, and limestone. Filled diamonds indicate the mass-based mixture proportions investigated in the paste portion of the present study.

axis indicate mixtures in which 10 % by mass of either a 100 % Type I OPC (right point at cement=90) or an ASTM C150 Type I/II with interground limestone cement (left point at cement≈87) is replaced by limestone powder. The third filled diamond data point corresponds to a mixture that contains 20 % fly ash and 5 % fine limestone powder, replacing 25 % of an ASTM C150 Type III with interground limestone cement. In addition, for a subset of these mixtures, both the surface area/particle size and the crystalline form (aragonite or calcite) of the limestone powder are investigated in studies on pastes. For the 10 % limestone mixtures, concretes are prepared, this time with a volumetric replacement of limestone powder for cement, and compared to a 100 % ASTM C150 Type I/II with interground limestone cement concrete mixture. Finally, this study of the influence of limestone on cement hydration and performance is extended to a larger length scale by considering the impact of aggregate type (limestone or siliceous) on concrete strength.

Materials and Procedures

Cements

Characteristics of the three cements employed in the various parts of this study, as supplied from their manufacturers' mill sheets, are provided in Table 1. The cements consisted of an ASTM C150 Type III cement, a white Type I cement, and a Type I/II cement. The Type III and Type I/II cements, while both meeting ASTM C150 specifications [1], each contained a

percentage of limestone powder added directly to the cement clinker prior to the grinding process (interground limestone) as indicated in Table 1. Particle size distributions, characterized by their particle size parameters D_{10} , D_{50} , and D_{90} (representing the 10th, 50th, and 90th percentile, respectively) in Table 1, were determined using laser diffraction equipment, with isopropanol as the dispersant. The particle size parameters in Table 1 are determined by averaging six separate scans, with a typical coefficient of variation being less than 1 %.

Table 1. Characteristics of cements employed in the study (percentages by mass)

| | Type III cement | White (Type I) cement | Type I/II cement |
|--------------------------------|-------------------------|-------------------------|-------------------------|
| SiO ₂ | 18.56 % | 24.26 % | 19.7 % |
| Al ₂ O ₃ | 5.7 % | 2.08 % | 4.9 % |
| Fe ₂ O ₃ | 2.16 % | 0.31 % | 3.4 % |
| CaO | 62.27 % | 68.58 % | 62.0 % |
| MgO | 2.35 % | 0.58 % | 3.0 % |
| SO ₃ | 4.47 % | 2.14 % | 3.0 % |
| CO ₂ | 1.58 % | - | 1.24 % |
| LOI | 2.49 % | 1.04 % | 2.6 % |
| Total alkalis ^A | 1.03 % | 0.19 % | 0.54 % |
| Limestone addition | 3.82 % | - | 2.94 % |
| Blaine fineness | 481 m ² /kg | 397 m ² /kg | 373 m ² /kg |
| Density | 3 070 kg/m ³ | 3 140 kg/m ³ | 3 270 kg/m ³ |
| D ₁₀ | 1.32 μm | 1.41 μm | 2.18 μm |
| D ₅₀ | 10.6 μm | 9.85 μm | 11.9 μm |
| D ₉₀ | 30.8 μm | 34.6 μm | 35.8 μm |

^ANa₂O+0.658*K₂O

Limestones

Two of the limestone powders employed in this study, including the finest material, were supplied by OMYA¹, while the other two were obtained from Specialty Minerals (SM), including a precipitated calcium carbonate (PCC - denoted as Sturcal F) powder based on the aragonite polymorph of CaCO₃, as opposed to calcite. In Table 2, limestone powder densities (± 10 kg/m³ standard deviation) were measured using a helium pycnometer and their BET (Brunauer, Emmett, and Teller [13]) surface areas (coefficient of variation of 2 % for three replicate specimens [9]) were measured using nitrogen adsorption. A sample of the aragonite-based Sturcal F limestone powder was subsequently heat treated (HT) at 480 °C \pm 10 °C for 4 h to thermally convert the aragonite polymorph to calcite [14]. The converted powder was then evaluated both in a white cement mixture and in a cement/fly ash blend.

Pastes Studies

To investigate potential mixture modifications for a pre-cast operation, pastes were prepared using each of the four original and the heat-treated limestone powders in combination with either the Type I white cement or a blend of the Type III cement and a Class F fly

¹ Certain commercial products are identified in this paper to specify the materials used and the procedures employed. In no case does such identification imply endorsement or recommendation by the National Institute of Standards and Technology, the Federal Highway Administration, the National Research Council Canada, or Purdue University, nor does it indicate that the products are necessarily the best available for the purpose.

Table 2. Characteristics of limestone powders employed in the study

| Limestone Source | Composition | Density | BET surface area | D ₁₀ | D ₅₀ | D ₉₀ |
|---------------------------|--|-------------------------|--|-----------------|-----------------|-----------------|
| OMYA (fine) | 98 % CaCO ₃ ^A | 2 710 kg/m ³ | 9.93 m ² /g | 0.64 μm | 1.58 μm | 4.89 μm |
| OMYA (coarse) | 95 % CaCO ₃ ^A | 2 710 kg/m ³ | 0.83 m ² /g | 1.91 μm | 15.7 μm | 60.1 μm |
| SM Marblewhite | 96 % CaCO ₃ ^A 98.1 % calcite ^B | 2 740 kg/m ³ | 1.29 m ² /g | 1.36 μm | 7.11 μm | 16.2 μm |
| SM Sturcal F | 74.7 % aragonite 25.3 % calcite ^B | 2 760 kg/m ³ | 6 m ² /g ^C 5.60 m ² /g | 1.07 μm | 3.09 μm | 11.0 μm |
| Heat-treated SM Sturcal F | 1.5 % aragonite 98.5 % calcite ^B | 2 600 kg/m ³ | 3.52 m ² /g | 1.59 μm | 4.42 μm | 12.2 μm |

^{A,C}Reported by manufacturer (^Aassumed to be calcite).

^BX-ray diffraction (Rietveld method) determination at NIST (standard deviation ≤ 0.2 %).

ash (ASTM C618 [15]). The Class F fly ash has a density of 2 610 kg/m³ and D₁₀, D₅₀, and D₉₀ values of 2.46 μm, 18.3 μm, and 72.6 μm, respectively, thus being the coarsest of the powder materials used in the study. For this paste study, the water-to-powder ratio (*w/p*) by mass was maintained at 0.38 (typical of pre-cast concrete) and all substitutions of limestone for cement were made on a mass basis, to mimic current industry practice. The base blended mixture currently used in a pre-cast operation is an 85/15 mass blend of the Type III cement and the Class F fly ash. Mixture modifications consisted of increasing the fly ash to 20 % and replacing an additional 5 % of the Type III cement with each of the limestone powders. For the white cement mixtures, 10 % of the cement by mass was replaced with each limestone powder. Pastes were prepared at 25 °C using a water-cooled high shear blender and evaluated for initial setting time, using an automated Vicat apparatus (ASTM C191 [16]), and both isothermal (23 °C) and semi-adiabatic calorimetry. The specimens for semi-adiabatic calorimetry were prepared with a constant specimen volume of 150 cm³. Isothermal calorimetry assesses material reactivity, while the semi-adiabatic response can be more indicative of the field performance to be expected in the casting bed at a pre-cast production plant. The ASTM C191 test method [16] reports a single-operator standard deviation of 12 min for initial setting time, for the range of 49 min to 202 min. For isothermal calorimetry, using similar materials, the average absolute difference between replicate specimens has been measured to be 2.5 x 10⁻⁵ W/g (cement), with a maximum absolute difference of 0.00011 W/g (cement) for measurements conducted between 1 h and 7 d after mixing [17].

Concrete Mixtures with Volumetric-based Limestone Replacement for Cement

Using the Type I/II cement, concretes were prepared at the Federal Highway Administration's Turner Fairbanks Highway Research Center (TFHRC) laboratory, according to the procedures provided in ASTM C192 [18]. In addition to a 100 % cement control mixture, mixtures were prepared with either a fine (1.6 μm) or a coarse (16 μm) limestone powder replacing 10 % of the cement by volume. Concrete mixture proportions are provided in Table 3 and a constant dosage of high range water reducing agent (HRWRA) was employed throughout. In addition to characterizing fresh properties (temperature, slump, etc.), the following measurements were performed: initial and final setting times (ASTM C403 [19]) on a sieved mortar fraction of the concrete (ASTM C172 [20]), compressive strengths (ASTM C39 [21]) at 1 d, 3 d, 28 d, and 56 d, rapid chloride permeability test (RCPT – ASTM C1202 [22]) at 56 d, and surface resistivity at 56 d (modified AASHTO TP95 [23]). Additionally, isothermal

calorimetry was measured during the course of 7 d on a portion of the sieved mortar fraction. The ASTM C403 test method [20] reports single-operator coefficients of variation for times of initial and final setting of 7.1 % and 4.7 %, respectively.

Table 3. Mixture proportions for concrete mixtures with and without 10 % limestone powder replacing cement on a volume basis

| Material | 100 % OPC | 10 % 1.6 μm limestone | 10 % 16 μm limestone |
|------------------|------------------------------|----------------------------------|---------------------------------|
| Cement | 335 kg/m^3 | 302 kg/m^3 | 302 kg/m^3 |
| Limestone | --- | 28 kg/m^3 | 28 kg/m^3 |
| Coarse aggregate | 1 040 kg/m^3 | 1 040 kg/m^3 | 1 040 kg/m^3 |
| Fine aggregate | 858 kg/m^3 | 858 kg/m^3 | 858 kg/m^3 |
| Water | 134 kg/m^3 | 134 kg/m^3 | 134 kg/m^3 |
| HRWRA | 1 675 mL/m^3 | 1 675 mL/m^3 | 1 675 mL/m^3 |
| w/p | 0.400 | 0.406 | 0.406 |

Studies of Limestone vs. Siliceous Aggregates

As the final part of the current study, limestone and siliceous aggregates from the same respective batches that had been previously used to prepare laboratory concretes (limestone concretes had been prepared at Purdue University and siliceous concretes at TFHRC) were obtained for evaluation of their elastic modulus and image-based dimensions, using an Aggregate Image Measurement System (AIMS). The coarse aggregates were washed, sieved, and sorted by size. The 9.5 mm to 12.7 mm size fraction was used to prepare composite beam specimens (25 mm by 25 mm by 255 mm) for measurement of their modulus using resonant frequency techniques [24]. Microsere 5714A wax (melting point of 70 °C) or a two-component epoxy was used as the binder for these composite beams. The wax was melted in the top pan of a double boiler, poured into Plexiglass beam molds that were either empty or contained a packed bed of the aggregates, and its top surface smoothed to prepare the beam. The beams with the epoxy were prepared by injection into the molds. The aggregate and wax/epoxy volume fractions in the composite were directly determined from mass and dimension measurements and the known densities of the aggregates (limestone – 2 750 kg/m^3 , siliceous – 2 570 kg/m^3). At least ten resonant frequency measurements were performed on each beam and the median value, converted to a Young’s modulus using the equations provided in the standard [24], was used to characterize each specimen’s response. In the analysis of the modulus data, the following values of Poisson’s ratio were assumed for the different components: limestone = 0.3, siliceous aggregates = 0.2, wax = 0.4, epoxy = 0.3 [25].

Coarse aggregates’ shape and texture were characterized using the aggregate imaging analysis system (AIMS2, a second generation of AIMS) originally developed by Masad [26]. The system uses a digital camera mounted to a variable magnification microscope, providing a maximum field of view of 53.7 mm x 71.6 mm (0.044 mm per pixel) down to a field of view of 4 mm x 5.4 mm (0.0033 mm per pixel). Backlighting is used in order to capture particle silhouettes for angularity analysis, while oblique top lighting is used to capture surface features in black and white images for texture analysis. The two dimensional angularity images are also used to capture the overall particle dimensions along the major (longest) and minor (shortest) axes. The third particle dimension is established by the position of the focal plane determined while capturing the texture image at the surface of the particle. The gradient vector and wavelet analysis methods are used to quantify angularity and surface texture, respectively [26].

Results and Discussion

Paste Studies

For the paste investigations, both the particle size/surface area of the limestone powder and two polymorphs of CaCO_3 , aragonite and calcite, were investigated. As indicated in Table 4, the 1.6 μm limestone powder was able to maintain or reduce the initial setting time relative to a corresponding control paste without limestone powder. The coarser limestone powders were less effective in reducing setting times, with the aragonite form (Sturcal F) actually prolonging the initial setting time in the cement/fly ash blend. The initial setting time measurements are reinforced by the isothermal (23 °C) and semi-adiabatic calorimetry results presented in Figures 2 to 5. In a typical isothermal calorimetry curve for portland cement hydration, following an induction period of little thermal activity, the first peak generally corresponds to hydration of the silicate phases, mainly the more reactive tricalcium silicate phase, while the second peak or subsequent shoulder indicates a renewed reaction of the aluminate phases, generally present in the tricalcium aluminate and tetracalcium aluminoferrite phases [27]. Naturally, the white cement has a very low ferrite content (Table 1), so that nearly all of its aluminate reactions are due to the tricalcium aluminate phase that it contains.

Table 4. Initial setting times of Type III/F ash/limestone ternary and white cement/limestone blends ($w/p=0.38$ by mass for all mixtures)

| Cement Mixture | Initial Setting Time |
|---|-----------------------------|
| 85 % Type III cement/15 % Class F fly ash | 3.3 h |
| 75 % Type III cement/25 % Class F fly ash | 3.8 h |
| 75 % Type III cement/20 % F ash/5 % 1.6 μm limestone | 3.3 h |
| 75 % Type III cement/20 % F ash/5 % 16 μm limestone | 3.7 h |
| 75 % Type III cement/20 % F ash/5 % Marblewhite limestone | 3.6 h |
| 75 % Type III cement/20 % F ash/5 % Sturcal F limestone | 4.1 h |
| 100 % white cement | 4.2 h |
| 90 % white cement, 10 % 1.6 μm limestone | 3.7 h |
| 90 % white cement, 10 % 16 μm limestone | 4.3 h |
| 90 % white cement, 10 % Marblewhite limestone | 4.0 h |
| 90 % white cement, 10 % Sturcal F limestone | 4.2 h |

The contrast between the effects of the calcite and aragonite polymorphs of calcium carbonate can be seen in the isothermal calorimetry curves in Figures 2 and 3. The limestone powders based on calcite both accelerate (speed up) and amplify (increase the intensity of) the silicate reactions in both the cement/fly ash blend (Figure 2) and the white cement (Figure 3) systems, most likely by providing additional surfaces for the precipitation of early-age hydration products [28]. By contrast, little if any acceleration/amplification of the silicate peak is observed for the original Sturcal F, aragonite-based CaCO_3 . Atomic force microscopy (AFM) studies have indicated that the surface structures of calcite and aragonite (for their most common cleavage planes) in aqueous solutions are significantly different from one another [29,30]. The calcite surfaces consist of a planar configuration of Ca and O atoms, perhaps not unlike the CaO layers in a conventional calcium silicate hydrate gel (C-S-H). The measured spacing of the calcium atoms in their grid on the calcite (10 $\bar{1}$ 4) cleavage plane, 0.5 nm by 0.4 nm [29], is not that different from the 0.56 nm by 0.36 nm spacing mentioned for the CaO layers in 1.4-nm

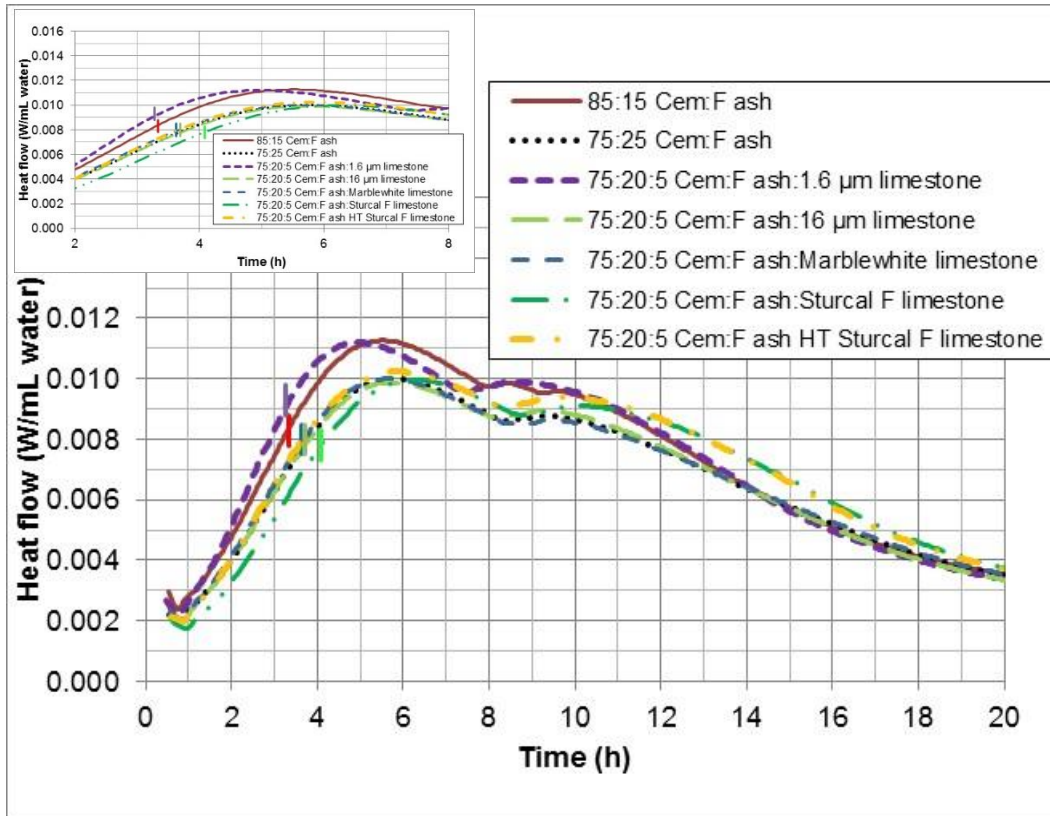


Figure 2. Isothermal heat flow as a function of time at 23 °C for Type III cement/F ash with and without various limestone replacements. Short vertical lines for each curve between 3 h and 4 h indicate initial setting time for that mixture. Inset shows a zoom of the 2 h to 8 h data.

tobermorite (similar to C-S-H) structures [27]. Conversely, in aragonite, only Ca atoms are detected on the surface layer, with no indication of the presence of corresponding O atoms [30]. Based on the calorimetry results here, the surface of calcite is more favorable for the precipitation and growth of early-age C-S-H (and perhaps other hydration products) than that provided by the aragonite polymorph of CaCO_3 . The semi-adiabatic temperature rise curves shown in Figures 4 and 5 are consistent with these isothermal calorimetry results, as in both systems, the aragonite-based CaCO_3 produced a significant retardation in measured temperature rise in comparison to all of the other mixtures.

Although the surface structures of aragonite and calcite are different, their room temperature solubilities in water are quite similar. Specifically, at 25 °C, Plummer and Busenberg [31] measured $\log(K_{sp})$ values of -8.480 ± 0.020 and -8.336 ± 0.020 , for calcite and aragonite, respectively, for the dissolution of CaCO_3 to form Ca^{2+} and CO_3^{2-} ions. The dissolved carbonate ions can participate in the hydration reactions, particularly those of the aluminate phases, leading to the formation of carboaluminates as opposed to sulfoaluminates, and also stabilizing the ettringite that is produced at early ages [32,33]. These carboaluminates are both more voluminous [32,34] and potentially stiffer [35] than their corresponding sulfoaluminates, leading to further reductions in system porosity and increases in measured strengths. With similar solubilities, it not surprising that both polymorphs of CaCO_3 are quite effective at accelerating and amplifying the aluminate reactions, as indicated by the second peak/shoulder in the isothermal calorimetry curves in Figures 2 and 3. The efficacy of the limestone powders in

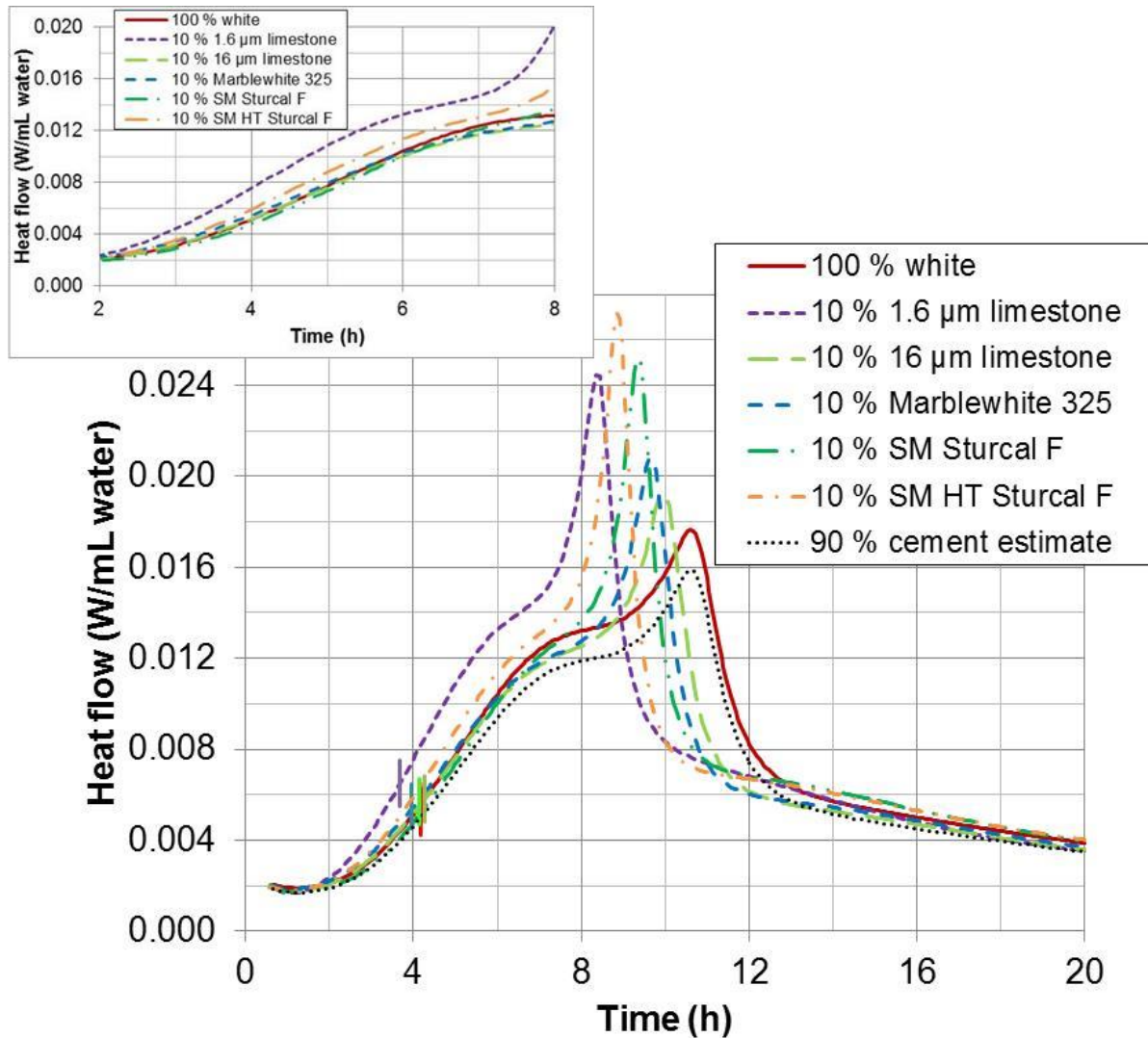


Figure 3. Isothermal heat flow as a function of time at 23 °C for white cement with and without various 10 % limestone replacements. The 90 % cement estimate is provided as an indication of the expected result due to simple dilution of the cement content.

this regard is particularly noticeable in the case of the white cement in Figure 3, where in several cases, the height of this peak is increased by nearly 50 % relative to the value obtained for the 100 % white cement paste.

To further investigate the influence of CaCO_3 polymorphs on cement hydration, the Sturcal F powder was heat treated (denoted as HT Sturcal F) at $480 \text{ °C} \pm 10 \text{ °C}$ for 4 h [13]. The changes that the heat treatment produced in the PSD and x-ray diffraction patterns are provided in Figures 6 and 7, respectively. While the PSD was coarsened (perhaps partially due to agglomeration), the density slightly lowered, and the surface area somewhat reduced (Table 2), the conversion of aragonite to calcite, as verified by the disappearance of the aragonite peaks in the heat-treated Sturcal F's x-ray diffraction patterns in Figure 7, was indeed successful in increasing the acceleration/amplification provided by the limestone powder, particularly with respect to the early-age silicate reactions in both the cement/fly ash blend and in the white cement mixture (Figures 2 and 3) and with respect to the aluminat reactions in the white cement

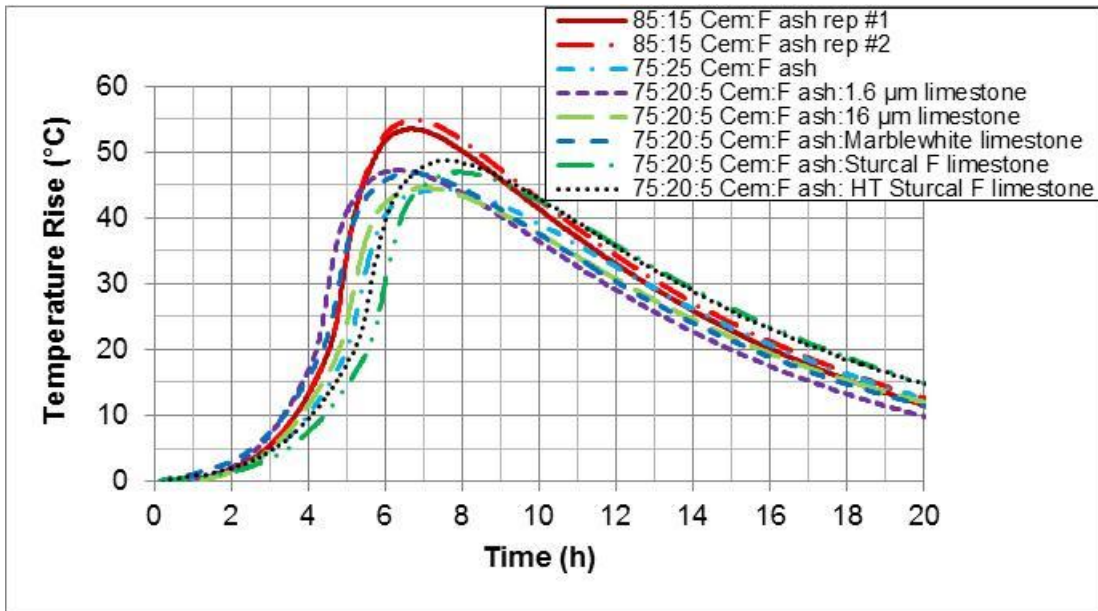


Figure 4. Semi-adiabatic temperature rise of Type III cement/F ash pastes with and without various limestone replacements. Separate results from two replicate specimens for the base mixture (85:15 Cem:F ash) are shown to provide an indication of variability.

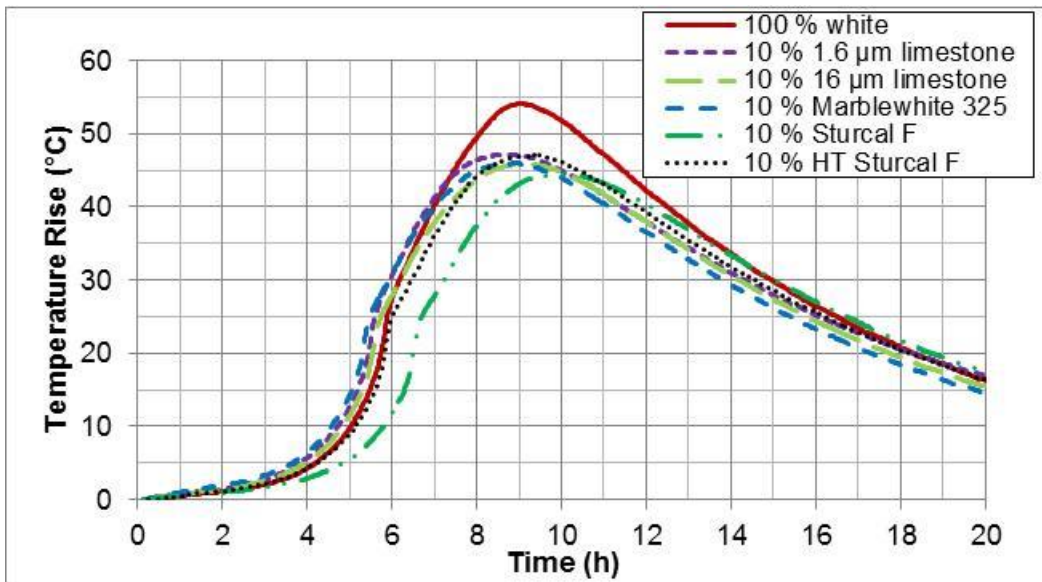


Figure 5. Semi-adiabatic temperature rise of white cement pastes with and without various 10% limestone replacements.

mixture (Figure 3). Additionally, nearly all of the retardation in the semi-adiabatic temperature rise curves (Figures 4 and 5) was removed via the heat treatment applied to the Sturcal F powder. While the volumetric heat capacity of aragonite is about 6.7% higher than that of calcite [36], since replacements were made on a mass basis and semi-adiabatic specimens were of a constant volume in this study, the calculated thermal capacity difference between the two mixtures with original and heat-treated Sturcal F is less than 0.5%. This suggests that the restoration of the semi-adiabatic temperature rise response in the specimen with the heat-treated Sturcal F was

mainly due to altering the reactivity of the CaCO_3 in the cementitious systems, as opposed to a significant change in thermal properties (e.g., heat capacity).

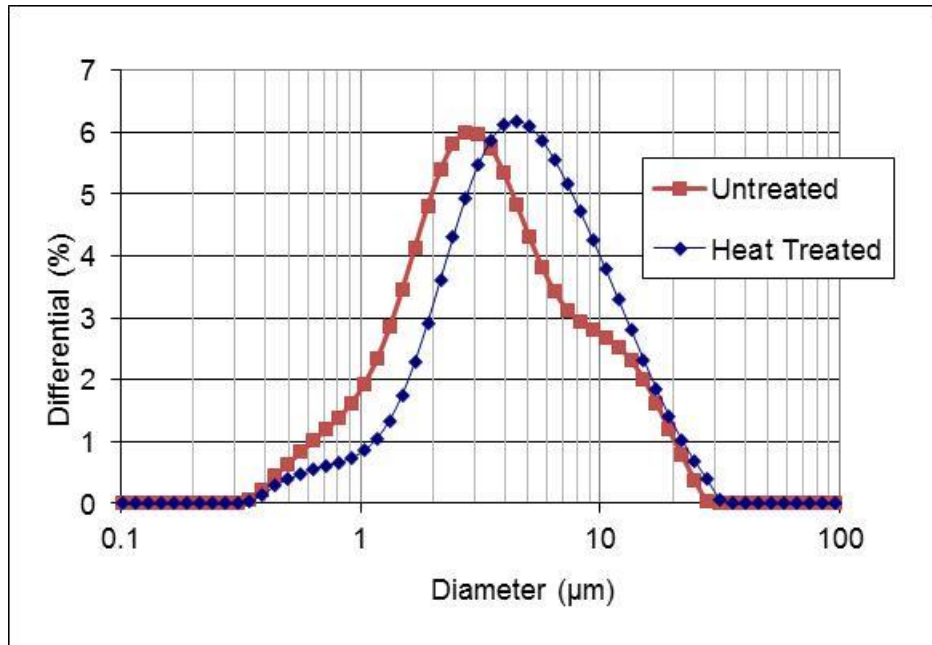


Figure 6. Measured particle size distributions for Sturcal F limestone powder before and after heat treatment at 480 °C for 4 h.

The subsequent fate of calcite particles immersed in water has also been studied using AFM techniques by several research groups [37,38]. In general, these researchers have observed that a hydrate layer of up to four layers of water (~ 0.5 nm thick) can form on the calcite surface and also observed the formation of “broad and shallow” etched pits, achieving equilibrium during the first 15 min or so of immersion. The localized precipitation of C-S-H gel and other hydration products on calcite surfaces during the hydration of tricalcium silicate has been directly observed by Sato and colleagues [39] using scanning electron microscopy (SEM) and one time series representation of four such images is provided in Figure 8. Initially, a very ordered pattern of precipitated material on the surface of the CaCO_3 particles is observed, consistent with the ordered arrangement of Ca and O atoms on calcite cleavage surfaces observed via AFM [29]. The images in Figure 8 could be compatible with the hypothesis that the initially formed hydrated etch pits could subsequently serve as the original precipitation sites for C-S-H gel during early-age hydration. These sites may be even more favorable for precipitation and growth of C-S-H gel than those provided by the tricalcium silicate or cement particles themselves [11,12,39].

Concrete Mixtures

The ability of the limestone powders to accelerate early-age hydration in pastes was also observed in the laboratory concretes prepared at TFHRC. Figure 9 provides the isothermal calorimetry curves measured at 25 °C for mortars sieved from the three concrete mixtures. Once again, the finer limestone is seen to accelerate and amplify both the early-age silicate and aluminate phase reactions. Due to its reduced surface area (both for precipitation of phases and for dissolution of CaCO_3 to generate CO_3^{2-} ions), the acceleration and amplification provided by

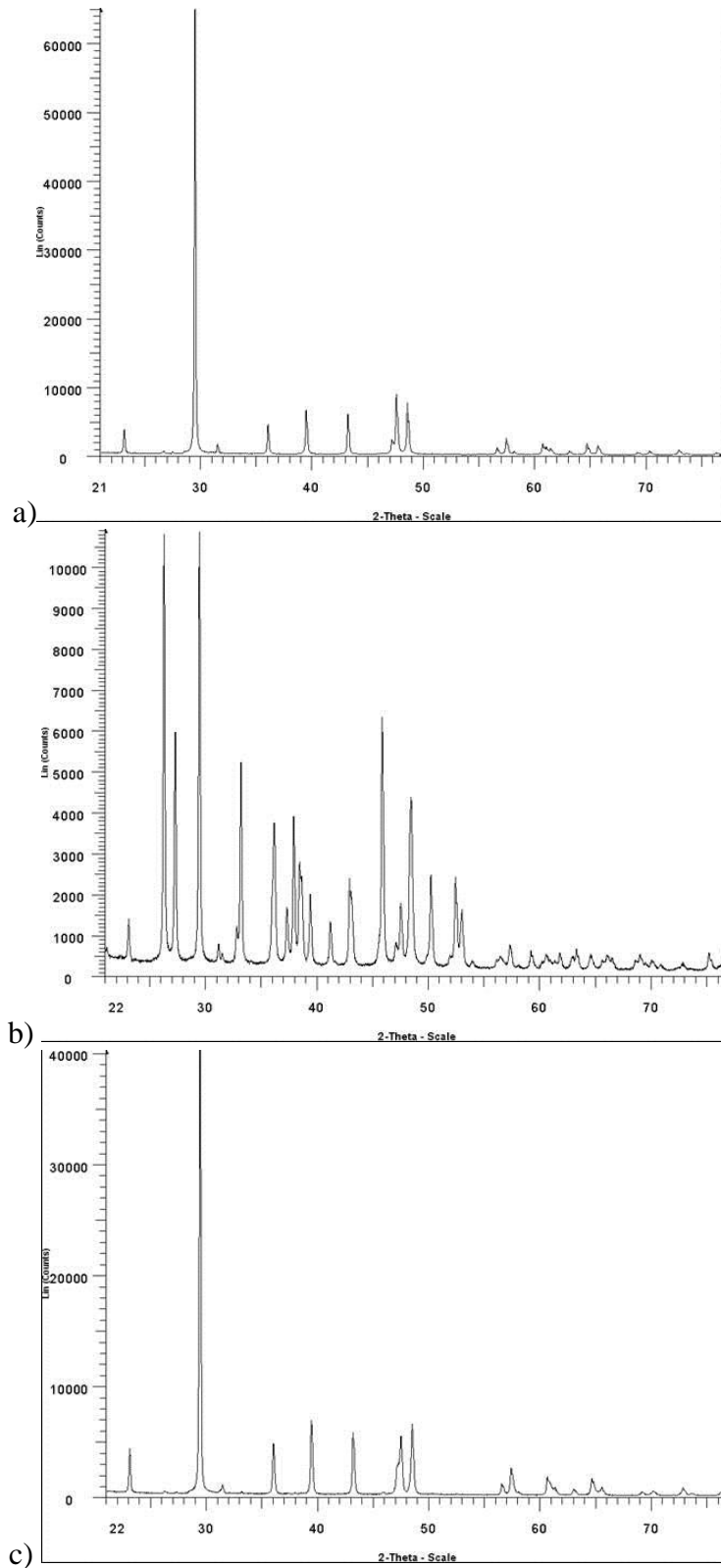


Figure 7. X-ray diffraction patterns for a) Marblewhite, b) original Sturcal F, and c) heat-treated Sturcal F limestone powders. See Table 2 for quantitative Rietveld analysis.

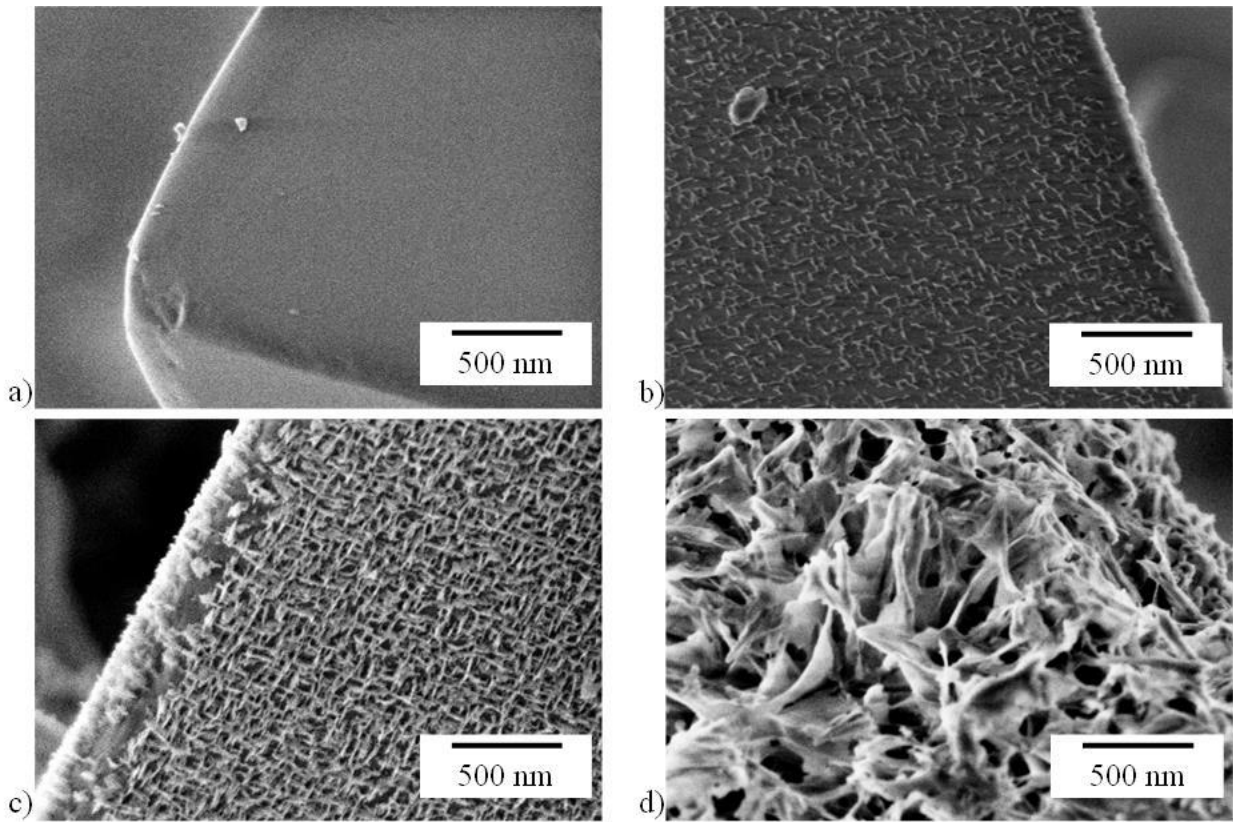


Figure 8. Scanning electron microscopy images of limestone surfaces during hydration with C_3S at a) 0 h, b) 1 h, c) 4 h, and d) 28 d.

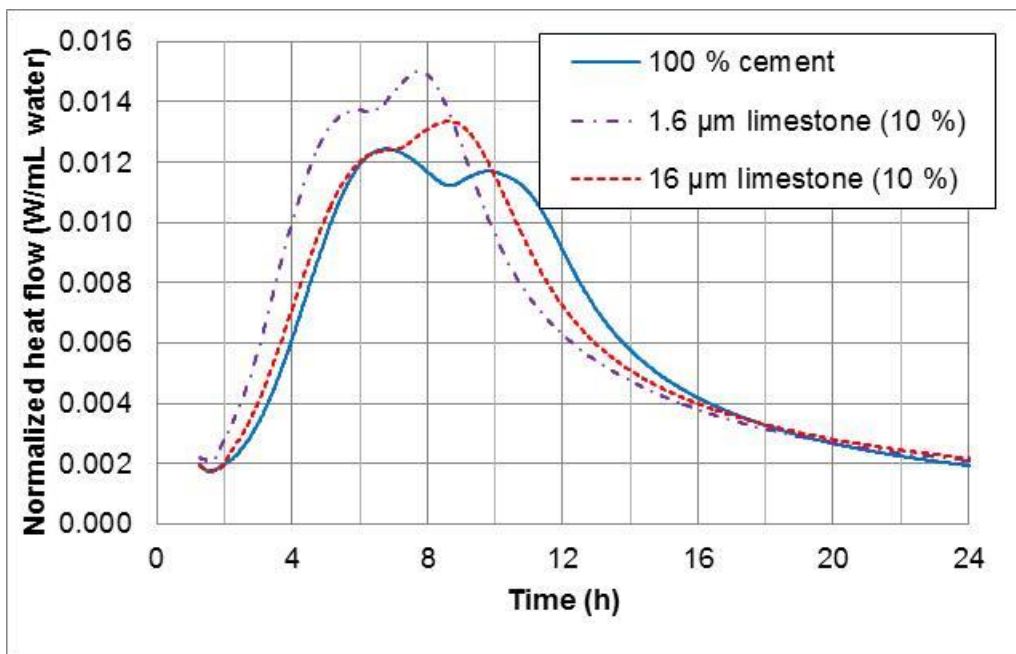


Figure 9. Isothermal heat flow as a function of time at 25 °C for mortars sieved from batched concretes prepared with and without 10 % limestone powder replacements for cement by volume.

the coarser limestone is less, but still significant considering that 10 % of the cement by volume has been removed from the system. The acceleration/amplification provided by the finer limestone is further confirmed by the comparison of the setting times provided in Table 5, where the 1.6 μm limestone decreased both the initial and final setting times in comparison to those of the 100 % cement control concrete. In terms of compressive strength, mainly due to their 10 % cement dilution, the limestone-containing concretes were not able to maintain the strength levels of the 100 % cement control at later ages, but each still achieved a nominal 28 d compressive strength of 40 MPa, with a further increase of about 4 MPa between 28 d and 56 d. By further comparison, their transport properties, as characterized by measurements of both RCPT and surface resistivity at 56 d, were nominally equivalent or measurably better than those of the 100 % cement concrete. Further performance benefits of these fine limestone powder additions have been observed recently in ternary blends of cement, fly ash, and limestone, including a series of high volume fly ash concrete mixtures with clinker content reductions between 40 % and 60 % [10].

Table 5. Properties of TFHRC concrete mixtures with or without 10 % limestone powder

| Mixture | Time of initial set | Time of final set | 1-d strength | 3-d strength | 28-d strength | 56-d RCPT | 56-d resistivity |
|----------------------------------|---------------------|-------------------|------------------------------------|-----------------------|--|--------------------|--|
| OPC control | 3.73 h | 5.20 h | 19.8 MPa (0.1 MPa) ^A | 28.8 MPa (0.3 MPa) | 46.5 MPa (0.3 MPa) | 2 470 C (130 C) | 7.0 k Ω ·cm (0.7 k Ω ·cm) |
| 10 % 1.6 μm limestone | 3.17 h | 4.63 h | 17.9 MPa (0.4 MPa) | 29.3 MPa (1.3 MPa) | 40.8 MPa (0.4 MPa) 56 d 44.5 MPa | 2 390 C (50 C) | 7.8 k Ω ·cm (0.1 k Ω ·cm) |
| 10 % 16 μm limestone | 4.00 h | 5.50 h | 17.6 MPa (0.2 MPa) | 29.1 MPa (0.2 MPa) | 39.7 MPa (0.9 MPa) 56 d 42.8 MPa | 2 790 C (170 C) | 7.4 k Ω ·cm (0.4 k Ω ·cm) |

^ANumbers in parentheses indicate standard deviation for three replicate specimens for control mixture and for two replicate specimens for mixtures with limestone.

Studies of Limestone vs. Siliceous Aggregates

In the final portion of the study, the influence of larger aggregate-sized limestone on concrete performance was examined. Anecdotal evidence and a few direct comparative studies indicate that for otherwise equivalent concrete mixtures, limestone aggregates often produce higher compressive strengths than siliceous aggregates [40,41]. Typical strength improvements produced using limestone aggregate are from 10 % to 20 %, with enhancements generally observed at all ages from 1 d to 28 d. More recently, in the course of developing linear relationships between compressive strength and heat release (a measure of achieved hydration) [42], this same trend in strength enhancement has been observed for concretes prepared with limestone or siliceous aggregates, as shown in Figure 10 [10]. While the limestone and siliceous concretes were prepared at different laboratories, they had similar total aggregate volume fractions of 75 % for the limestone concrete and 74.4 % for the siliceous concrete. Once again, the strength enhancement is present at all levels of heat release (age) and for these mixtures is actually about 30 %, for strengths greater than 25 MPa.

French and Mokhtarzadeh [41] have attributed this strength enhancement to the fact that their limestone “exhibited a superior bond characteristic with cement paste and the plane of fracture in limestone concrete crossed most of the coarse aggregate particles. In contrast, round gravel particles showed poor bond with cement paste and, except for small-sized particles, the plane of fracture passed around coarse aggregate particles.” In addition to any physical/chemical

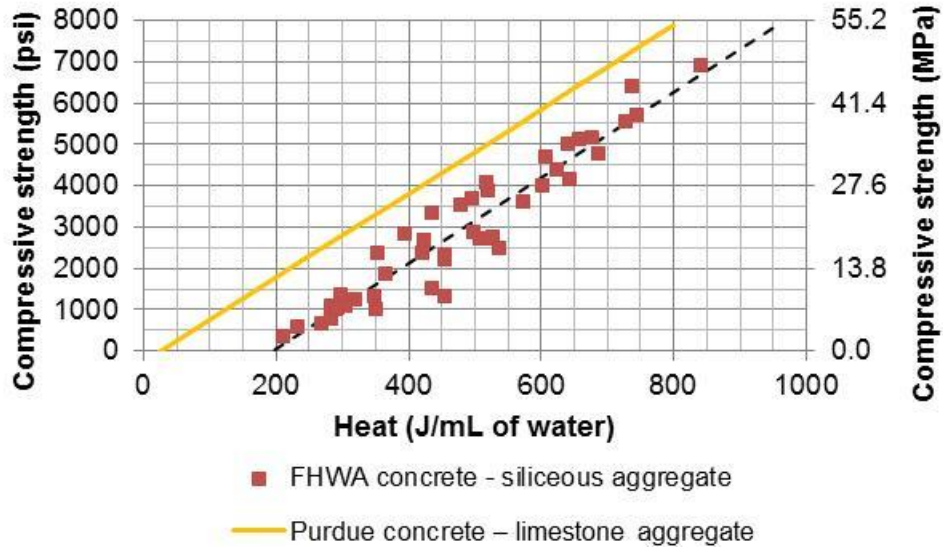


Figure 10. Measured concrete compressive strength as a function of the measured cumulative heat release (per unit volume of water) used to establish a strength-heat release linear relationship (dashed line, $R^2=0.91$) [10]. Purdue regression line was taken from [42].

bonding superiority of the limestone aggregate, another factor that must be considered is that the limestone aggregate could be stiffer (higher modulus) than the siliceous aggregate. In the rocks literature, the commonly reported ranges for elastic modulus for these two rock types overlap, so that one cannot conclude that one is always stiffer than the other. Therefore, the modulus measurements presented in Figure 11 were conducted to directly assess this possibility for the two aggregates used to prepare the concretes in Figure 10. In Figure 11, the measured composite modulus is plotted as a function of volume fraction of aggregates, along with an estimate of the individual aggregate modulus based on “fitting” the Hashin-Shtrikman (H-S) bounds [43] for a two-phase composite (aggregate-wax or aggregate-epoxy) to the experimental data. Solid lines are estimated H-S bounds for siliceous-wax composite with $E_{agg}=50$ GPa and $E_{wax}=2.43$ GPa, narrow dashed lines are H-S bounds for siliceous-epoxy composite with $E_{agg}=50$ GPa and $E_{epoxy}=3.73$ GPa, wide dashed lines are H-S bounds for limestone-wax composite with $E_{agg}=40$ GPa and $E_{wax}=2.43$ GPa, and dotted lines are H-S bounds for limestone-epoxy composite with $E_{agg}=40$ GPa and $E_{epoxy}=3.73$ GPa. While there was some variability in the individual resonant frequency measurements for each specimen, the median values shown in Figure 11 indicate the likelihood that the limestone aggregates have an elastic modulus that is equal to or slightly less than their siliceous counterparts. This further supports the claim of French and Mokhtarzadeh [41] that the strength enhancement is due to superior bonding and not to a stiffer aggregate. The limestone aggregate surfaces, while providing much less surface area than a fine limestone powder, should be equally favorable for precipitation and growth of early-age (and later age) hydration products, producing a superior interfacial transition zone bond with the hydrating cement paste [44,45]. This would be consistent with the strength increases observed with limestone aggregates beginning as early as 1 d (usually the first time of testing). Similar observations were provided recently in a study of supercritical carbonation of calcareous composites, where it was observed that “calcareous aggregates appear to augment the strength enhancement effected during supercritical carbonation by encouraging preferential precipitation of calcite at the binder-aggregate interface” [46]. The present observations are also consistent

with the numerical results of a recent study by Kamali- Bernard et al. [47], who concluded that “Among the three studied aggregates types (limestone, siliceous, and polycarbonate plastic), only very dense limestone ones may increase the mechanical characteristics of the composite. Because of their weak bond adherence, siliceous and more particularly plastic aggregates may decrease both the Young’s modulus and compressive strength.”

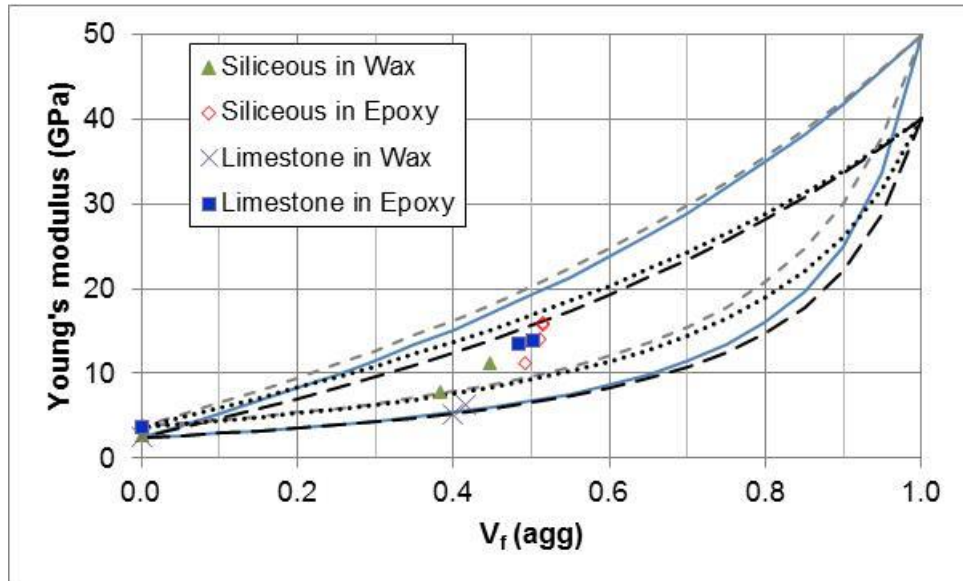


Figure 11. Measured elastic modulus data (points) for composite beams, along with the H-S upper and lower bounds as lines [43]. Two points (replicate measurement sets, often overlapping) are shown for the epoxy composite beams to provide an indication of variability.

In the present study, textural, shape, and angularity differences between the limestone and siliceous aggregates were also examined using the AIMS equipment. A summary of the obtained results is presented in Table 6, along with the measurement range for each AIMS parameter. The CAAT is a combined angularity texture value computed as 10 times the texture + one-half of the angularity. Example images of the 9.5 mm to 12.7 mm aggregates along with textural images obtained from the AIMS system are provided in Figure 12. The higher angularity, lower sphericity, coarser texture, and flatter and more elongated nature of the limestone aggregate could also be contributing to the enhanced bonding between paste and aggregate in concrete, in addition to the previously noted tendency for cement hydrates to precipitate on calcite surfaces. Further research investigating the relationship between AIMS parameters and concrete performance for a wider variety of aggregate sources is planned.

Table 6. AIMS-determined properties of aggregates

| Rock Type | Angularity (1-10000) | Sphericity (0-1) | Texture (0-1000) | Flat and Elongated Ratio > 2:1 | Flat or Elongated Ratio > 1:2 | CAAT (0-15000) |
|-----------|----------------------|------------------|------------------|--------------------------------|-------------------------------|----------------|
| Limestone | 3149 | 0.61 | 237 | 64.2 % | 34.2 % | 3945 |
| Siliceous | 2325 | 0.71 | 119 | 39.7 % | 13.5 % | 2353 |

While most natural deposits of limestone consist primarily of the mineral calcite, aragonite does exist in some locations, and the fine powder results on these two polymorphs

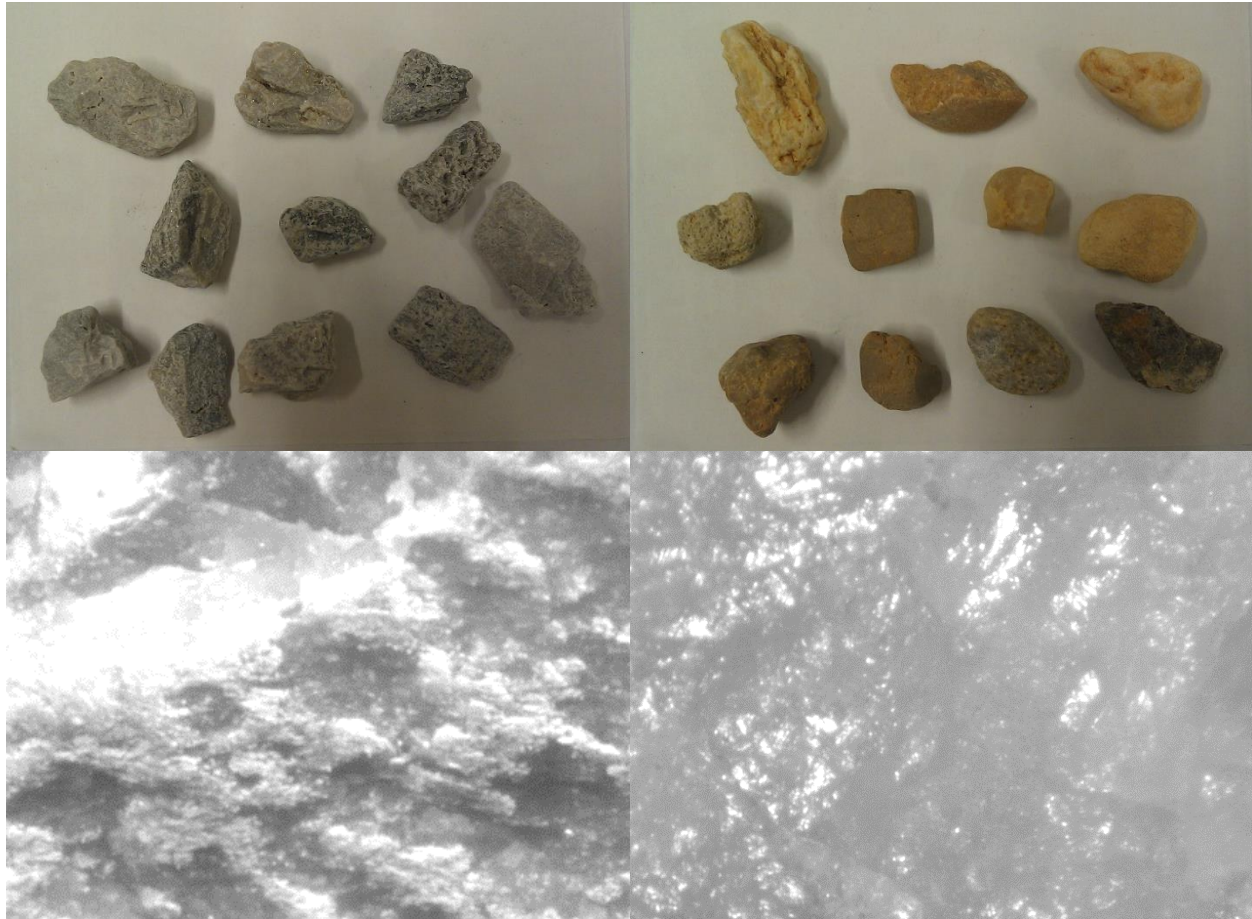


Figure 12: Photographs and images from AIMS analysis indicating general features for the 9.5 mm to 12.7 mm size range (top) and texture (bottom) for the 12.5 mm to 19.0 mm limestone (left) and for the 4.75 mm to 9.5 mm siliceous (right) aggregates. Top images are 100 mm wide by 75 mm high. Bottom images are 5.4 mm wide by 4.0 mm high.

presented earlier suggest that the bond between aragonite-based coarse aggregate and cement paste may not be as strong as that produced by the calcite-based limestone. In rare cases, this could contribute to the variable strength performance of concretes with “limestone” aggregates. Recent studies focused on reinforcing cement-based composites with aragonite-based CaCO_3 whiskers might also benefit from first thermally converting their aragonite polymorph to its calcite form [48]. Additionally, it is interesting to note that during the natural carbonation of concrete, both calcite and aragonite polymorphs can be produced, as well as vaterite and an amorphous form of CaCO_3 , depending on temperature, relative humidity, and exposure time [49]. This variation in carbonation product polymorphs could be one contributor to the observed variable impact of carbonation on the adhesion of cement-based repair materials to (carbonated) concrete [50], with calcite potentially promoting bond performance, while aragonite would likely reduce the adhesion/interfacial bond between the repair material and the existing substrate. Further investigation, perhaps using quantitative X-ray diffraction to evaluate the various polymorphs found in carbonated substrates [49], is required to verify this hypothesis.

Conclusions

This study has examined the performance of limestone in cement-based materials at multiple scales, highlighting the importance of the favorable surfaces provided by calcite for the precipitation and growth of hydration products. This both accelerates early-age hydration, reducing setting times, and improves the integrity and quality of the bond between limestone aggregates and hydrating cement paste in concrete, producing higher strengths. While the aragonite form of limestone does not provide a significant acceleration of the early-age silicate reactions, it is at least as soluble in water as calcite, with both providing ample carbonate ions to participate in cement hydration reactions that lead to enhanced aluminate reactivity, the stabilization of ettringite, and the formation of (more voluminous and potentially stiffer) carboaluminates in place of sulfoaluminates. The study has demonstrated that the thermal conversion of the aragonite polymorph of CaCO_3 to calcite can enhance its accelerating influence on the early-age silicate reactions. Because both the provision of surfaces for hydration product precipitation and the dissolution of CaCO_3 to provide carbonate ions are dependent on the surface area of the limestone powder, finer powders, such as the 1.6 μm median particle size powder employed in this study, provide an improved performance in comparison to coarser ones (16 μm for example). The physical and chemical interaction of limestone with the cement hydrates also likely contributes to the superior mechanical properties of concretes containing limestone aggregates in comparison to similar ones based on siliceous aggregates.

Acknowledgements

The authors thank IGI Specialty Materials and Enviro-Coatings, Lehigh Cement Company, OMYA Inc., Specialty Minerals Inc., and Unistress for providing materials for use in these studies. They would also to thank Dr. George Quinn of NIST for assistance with the resonant frequency measurements. The assistance of Dr. Haejin Kim, John Leavitt, and Senaka Samaranyake in helping to prepare and evaluate the concrete mixtures at TFHRC is gratefully acknowledged.

References

- 1) ASTM International, ASTM C150/C150M-12, Standard Specification for Portland Cement, ASTM International, West Conshohocken, PA, 9 pp., 2012.
- 2) ASTM International, ASTM C595/C595M-13, Standard Specification for Blended Hydraulic Cements, ASTM International, West Conshohocken, PA, 13 pp., 2013.
- 3) Barcelo, L., Blair, B., Delagrave, A., Innis, A., Knight, G., Thomas, M.D.A., and Weiss, W.J., "The Five Ws and One H of Portland Limestone Cement," *Concrete International*, **35** (11), 37-40, 2013.
- 4) Barcelo, L., Thomas, M.D.A., Cail, K., Delagrave, A., and Blair, B., "Portland Limestone Cement Equivalent Strength Explained," *Concrete International*, **35** (11), 41-47, 2013.
- 5) Thomas, M.D.A., Delagrave, A., Blair, B., and Barcelo, L., "Equivalent Durability Performance of Portland Limestone Cement," *Concrete International*, **35** (12), 39-45, 2013.
- 6) Hossack, A., Thomas, M.D.A., Barcelo, L., Blair, B., and Delagrave, A., "Performance of Portland Limestone Cement Concrete Pavements," *Concrete International*, **36** (1), 40-45, 2014.

- 7) Barrett, T., Sun, H., Villani, C., Barcelo, L., and Weiss, W.J., "Early-Age Shrinkage Behavior of Portland Limestone Cement," *Concrete International*, **36** (2), 51-57, 2014.
- 8) Bentz, D.P., Sato, T., de la Varga, I., and Weiss, W.J., "Fine Limestone Additions to Regulate Setting in High Volume Fly Ash Mixtures," *Cement and Concrete Composites*, **34** (1), 11-17, 2012.
- 9) Gurney, L., Bentz, D.P., Sato, T., and Weiss, W.J., "Reducing Set Retardation in High Volume Fly Ash Mixtures with the Use of Limestone: Improving Constructability for Sustainability," *Transportation Research Record, Journal of the Transportation Research Board*, No. 2290, Concrete Materials 2012, 139-146, 2012.
- 10) Bentz, D.P., Tanesi, J., and Ardani, A., "Ternary Blends for Controlling Cost and Carbon Content: High-Volume Fly Ash Mixtures Can Be Enhanced with Additions of Limestone Powder," *Concrete International*, **35** (8), 51-59, 2013.
- 11) Bentz, D.P., "Activation Energies of High-Volume Fly Ash Ternary Blends: Hydration and Setting," *Cement and Concrete Composites*, **53**, 214-223, 2014.
- 12) Oey, T., Kumar, A., Bullard, J.W., Neithalath, N., and Sant, G., "The Filler Effect: The Influence of Filler Content and Surface Area on Cementitious Reaction Rates," *Journal of the American Ceramic Society*, **96** (6), 1978-1990, 2013.
- 13) Brunauer, S., Emmett, P.H., and Teller, E., "Adsorption of Gases in Multimolecular Layers," *Journal of the American Chemical Society*, **60**, 309-319, 1938.
- 14) Yoshioka, S., and Kitano, Y., "Transformation of Aragonite to Calcite through Heating," *Geochemical Journal*, **19**, 245-249, 1985.
- 15) ASTM International, ASTM C618-12a, Standard Specification for Coal Fly Ash and Raw or Calcined Natural Pozzolan for Use in Concrete, ASTM International, West Conshohocken, PA, 5 pp., 2012.
- 16) ASTM International, ASTM C191-13, Standard Test Methods for Time of Setting of Hydraulic Cement by Vicat Needle, ASTM International, West Conshohocken, PA, 8 pp., 2013.
- 17) Bentz, D.P., and Ferraris, C.F., "Rheology and Setting of High Volume Fly Ash Mixtures," *Cement and Concrete Composites*, **32** (4), 265-270, 2010.
- 18) ASTM International, ASTM C192/C192M-13a, Standard Practice for Making and Curing Concrete Test Specimens in the Laboratory, ASTM International, West Conshohocken, PA, 8 pp., 2013.
- 19) ASTM International, ASTM C403/C403M-08, Standard Test Method for Time of Setting of Concrete Mixtures by Penetration Resistance, ASTM International, West Conshohocken, PA, 7 pp., 2008.

- 20) ASTM International, ASTM C172/C172M-10, Standard Practice for Sampling of Freshly Mixed Concrete, ASTM International, West Conshohocken, PA, 3 pp., 2010.
- 21) ASTM International, ASTM C39/C39M-14, Standard Test Method for Compressive Strength of Cylindrical Concrete Specimens, ASTM International, West Conshohocken, PA, 7 pp., 2014.
- 22) ASTM International, ASTM C1202-12, Standard Test Method for Electrical Indication of Concrete's Ability to Resist Chloride Ion Penetration, ASTM International, West Conshohocken, PA, 7 pp., 2012.
- 23) AASHTO TP95-11, Standard Method of Test for Surface Resistivity Indication of Concrete's Ability to Resist Chloride Ion Penetration, American Association of State Highway and Transportation Officials, Washington, D.C., 2011.
- 24) ASTM International, ASTM C1259-14, Standard Test Method for Dynamic Young's Modulus, Shear Modulus, and Poisson's Ratio for Advanced Ceramics by Impulse Excitation of Vibration, ASTM International, West Conshohocken, PA, 17 pp. 2014.
- 25) Cease, H., Derwent, P.F., Diehl, H.T., Fast, J., and Finley, D., "Measurement of Mechanical Properties of Three Epoxy Adhesives at Cryogenic Temperatures for CCD Construction," Fermi Lab Report Fermilab-TM-2366-A, 19 pp., 2006.
- 26) Masad, E., "Aggregate Imaging System (AIMS): Basics and Applications," Report FHWA/TX-05/5-1707-01-1, 2005.
- 27) Taylor, H.F.W., Cement Chemistry, 2nd edition, Thomas Telford, 1997.
- 28) Bentz, D.P., "Modelling the Influence of Limestone Filler on Cement Hydration Using CEMHYD3D," *Cement and Concrete Composites*, **28** (2), 124-129, 2006.
- 29) Rode, S., Oyabu, N., Kobayashi, K., Yamada, H., and Kühnle, A., "True Atomic-Resolution Imaging of (1014) Calcite in Aqueous Solution by Frequency Modulation Atomic Force Microscopy," *Langmuir*, **25**, 2850-2853, 2009.
- 30) Araki, Y., Tsukamoto, K., Oyabu, N., Kobayashi, K., and Yamada, H., "Atomic-Resolution Imaging of Aragonite (001) Surface in Water by Frequency Modulation Atomic Force Microscopy," *Japanese Journal of Applied Physics*, **51**, 08KB09, 2012.
- 31) Plummer, L.N., and Busenberg, E., "The Solubilities of Calcite, Aragonite, and Vaterite in CO₂-H₂O Solutions between 0 and 90 °C, and an Evaluation of the Aqueous Model for the System CaCO₃-CO₂-H₂O," *Geochimica et Cosmochimica Acta*, **46** (6), 1011-1040, 1982.
- 32) Matschei, T., Lothenbach, B., and Glasser, F.P., "The Role of Calcium Carbonate in Cement Hydration," *Cement and Concrete Research*, **37**, 551-558, 2007.

- 33) Cost, V.T., Matschei, T., Shannon, J., and Howard, I.L., "Extending the Use of Fly Ash and Slag Cement in Concrete through the Use of Portland-Limestone Cement," Proceedings NRMCA International Concrete Sustainability Conference, 2014.
- 34) De Weerd, K., Ben Haha, M., Le Saout, G., Kjellsen, K.O., Justnes, H., and Lothenbach, B., "Hydration Mechanisms of Ternary Portland Cements Containing Limestone Powder and Fly Ash," *Cement and Concrete Research*, **41**, 279-291, 2011.
- 35) Moon, J., Oh, J.E., Balonis, M., Glasser, F.P., Clark, S.M., and Monteiro, P.J.M., "High Pressure Study of Low Compressibility Tetracalcium Aluminum Carbonate Hydrates $3\text{CaO}\cdot\text{Al}_2\text{O}_3\cdot\text{CaCO}_3\cdot 11\text{H}_2\text{O}$," *Cement and Concrete Research*, **42**, 105-110, 2012.
- 36) Robie, R.A., Hemingway, B.S., and Fisher, J.R., "Thermodynamic Properties of Minerals and Related Substances at 298.15 K and 1 Bar (10^5 Pascals) Pressure and at Higher Temperatures," U.S. Geological Survey Bulletin 1452, 456 pp., 1978.
- 37) Araki, Y., Tsukamoto, K., Takagi, R., Miyashita, T., Oyabu, N., Kobayashi, K., and Yamada, H., "Submerged Atomic Resolution Imaging of Hydration Structure on Calcite," presentation 17th International Conference on Crystal Growth and Epitaxy – ICCGE-17, 2013, available at <http://science24.com/paper/28975>, access verified Feb. 24, 2014.
- 38) Stipp, S.L.S., Eggleston, C.M., and Nielsen, B.S., "Calcite Surface Structure Observed at Microtopographic and Molecular Scales with Atomic Force Microscopy (AFM)," *Geochimica et Cosmochimica Acta*, **58** (14), 3023-3033, 1994.
- 39) Sato, T., and Daillo, F., "Seeding Effect of Nano- CaCO_3 on the Hydration of Tricalcium Silicate," *Transportation Research Record, Journal of the Transportation Research Board*, No. **2141**, 61-67, 2010.
- 40) Mehta, P.K., and Monteiro, P.J.M., *Concrete: Structures, Properties, and Materials*, 2nd ed., Prentice-Hall, 1993.
- 41) French, C.W., and Mokhtarzadeh, A., "High Strength Concrete: Effects of Materials, Curing and Test Procedures on Short-Term Compressive Strength," *PCI Journal*, **38** (3), 76-87, 1993.
- 42) Bentz, D.P., Barrett, T., de la Varga, I., and Weiss, W.J., "Relating Compressive Strength to Heat Release in Mortars," *Advanced Civil Engineering Materials*, **1** (1), 1-14, 2012, doi:10.1520/ACEM20120002.
- 43) Hashin, Z., and Shtrikman, S., "A Variational Approach to the Theory of the Elastic Behaviour of Multiphase Materials," *Journal of Mechanics and Physics of Solids*, **11**, 127-140, 1963.
- 44) Grandet, J., and Ollivier, J.P., "Etude de la Formation du Monocarboaluminate de Calcium Hydrate au Contact d'un Granulat Calcaire dans une Pate de Ciment Portland," *Cement and Concrete Research*, **10**, 759-770, 1980.

- 45) Monteiro, P.J.M., and Mehta, P.K., “Interaction between Carbonate Rock and Cement Paste,” *Cement and Concrete Research*, **16** (2), 127-134, 1986.
- 46) Farahi, E., Purnell, P., and Short, N.R., “Supercritical Carbonation of Calcareous Composites: Influence of Mix Design,” *Cement and Concrete Composites*, **43**, 12-19, 2013.
- 47) Kamali-Bernard, S., Keinde, D., and Bernard, F., “Effect of Aggregate Type on the Concrete Matrix/Aggregates Interface and Its Influence on the Overall Mechanical Behavior. A Numerical Study,” *Key Engineering Materials*, **617**, 14-17, 2014.
- 48) Cao, M., Wei, J., and Wang, L., “Serviceability and Reinforcement of Low Content Whisker in Portland Cement,” *Journal of Wuhan University of Technology – Materials Science Edition*, 749-753, Aug. 2011.
- 49) Morandea, A., Thiery, M., and Dangla, P., “Investigation of the Carbonation Mechanism of CH and C-S-H in Terms of Kinetics, Microstructure Changes, and Moisture Properties,” *Cement and Concrete Research*, **56**, 153-170, 2014.
- 50) Bissonnette, B., Vaysburd, A.M., and von Fay, K.F., “Best Practices for Preparing Concrete Surfaces Prior to Repairs and Overlays,” Report Number MERL 12-17, U.S. Department of the Interior, Denver, CO, 92 pp., May 2012.